Available online at www.sciencedirect.com
SCIENCE DIRECT®
Bioorganic & Medicinal Chemistry 12 (2004) 2163–2172
Bioorganic & Medicinal Chemistry

Solution structure of rifaximin and its synthetic derivative rifaximin OR determined by experimental NMR and theoretical simulation methods

Silvia Martini,* Claudia Bonechi, Gianfranco Corbini, Alessandro Donati and Claudio Rossi

Department of Chemical and Biosystem Sciences, University of Siena, Via Aldo Moro, 2-53100 Siena, Italy

Received 12 December 2003; accepted 20 February 2004

Abstract—The solution structure of rifaximin and its derivative rifaximin OR (open ring) was determined by combining NMR experimental results, theoretical simulation of two-dimensional NMR spectra by complete relaxation matrix analysis (CORMA), and molecular dynamics calculations.

In this study the structural rearrangements due to the opening of the aliphatic chain of rifaximin after the reduction process to form rifaximin OR were investigated.

Close spatial proximity of CH_3(14) and H28b protons detected by 2D-ROESY spectrum of rifaximin OR, which was not present in rifaximin and the down-field shift of CH_3(34) protons in rifaximin OR ^{1}H spectrum were crucial to understand the structural modifications, which occurred within the system. The aliphatic chain of rifaximin OR was found to be no longer symmetrical with respect to the aromatic moiety. Although no dramatic structural rearrangements were detected, the aliphatic chain moved toward CH_3(14), causing a reduction of the aromatic shielding contribution in particular on CH_3(34).
© 2004 Elsevier Ltd. All rights reserved.

1. Introduction

Structural analysis plays an important role in the studies of the biological and pharmacological properties of bioactive compounds. The determination of the conformation in solution can be very useful to better understand biological functions and behavior.[1–3]

Rifamycins are naphthalenic ansamycins made by a naphtho-quinonic system condensed to a furanone ring spanned by an ansa chain connecting two opposite sides of the aromatic moiety. Several rifamycin derivatives have been studied during the last decades by both X-ray diffraction, NMR techniques, and molecular dynamics simulations.[4–14] The interest in structural analysis of this class of compounds lies in their activity as inhibitors of DNA dependent RNA polymerases (DDRP) of a wide variety of organisms, such as bacteria, eukaryotes, and viruses.[15–17] A large number of rifamycin derivatives are known, generally differing in the substitution at positions 3 and 4 of the chromophore. Rifamycin B, which represents the original compound isolated, possesses no activity but can be easily oxidized to rifamycin O, which can form rifamycin S by hydrolysis.[17] Rifamycin SV and rifamycin S are the reduced and oxidized forms, respectively, of the reversible oxidation–reduction system, which involves two electrons. Rifampicine is a semisynthetic derivative of rifamycin SV, which showed a strong activity.[14] For the best of our knowledge, the inhibition processes are not known, since neither the structure of rifamycin–DDRP complex, nor the structure of isolated DDRP have been determined. Arora[14] developed a qualitative model to explain the mechanism of action of rifamycins, involving the formation of hydrogen bonds between the enzyme and four rifamycin oxygens (O1, O2, O9, and O10), which must have a specific conformation. In particular, the O9 and O10 pointing outside the pharmacore represents the structural characteristic needed for activity. Bacchi and co-workers[10,12] reported more recent comprehensive

Keywords: Rifaximin; NMR; Molecular dynamics; Complete relaxation; Matrix analysis; Selective {H}C-NOE.
* Corresponding author. Tel.: +39-0577234372; fax: +39-0577234177; e-mail: martinis@unisi.it

0968-0896/$ - see front matter © 2004 Elsevier Ltd. All rights reserved.
doi:10.1016/j.bmc.2004.02.027

studies on the structure–activity relationships of rifamycins, in which they show a detailed picture of the structurally known rifamycins. They clearly investigated the main structural modifications of the ansa chain of nonactive compounds compared to some active rifamycins. Through the analysis of the variance of the 17 ansa backbone torsion angles, they found that active compounds showed a well-defined common pattern, while nonactive molecules were more scattered. In particular, they compared the structures of rifamycin S and rifamycin O, which represent a typical active and a typical sterically constrained molecule. They found out that in rifamycin S the ansa mean plane was approximately perpendicular to the naphtho-quinone, the O1, O2, O9, and O10 atoms pointed out of the same side of the molecule and CH_3(34) was oriented toward the chromophore. On the contrary, in rifamycin O CH_3(34) was hindered by the oxolanone 4-substituent and O9 and O10 pointed toward the aromatic moiety. They also compared ^{1}H NMR data of rifamycin O and rifamycin B with those of rifamycins S and SV, pointing out the structural changes, which mainly consist of proton chemical shift variations passing from rifamycin S to rifamycin O regarding CH_3(34), H26, and H24. 'Unusual' chemical shift values were found in rifamycin S and SV in different solvents by Casey and Whitlock[11] almost two decades before Bacchi and co-worker's works, showing this methyl to be sitting over the benzenoid ring. This behavior was found to be diagnostic with regards to the structural modifications occurring in the ansa chain of rifamycins and their derivatives.

In this paper we investigate the conformational properties of rifaximin (Chart 1a) and its derivative, rifaximin OR (Chart 1b), which belongs to a more recent class of ansamycin derivatives. Rifaximin is obtained from rifamycin SV[18,19] by chemical modification of the naphtho-furanone moiety. It exerts antibiotic effects[20–22] (like rifamycin SV) and reverse transcriptases of oncogenic and HIV RNA-viruses.[17,23]

Rifaximin OR was obtained by selective electrolytic reduction of the aliphatic chain of rifaximin giving an open ring structure.[24] Previous studies of these compounds showed the existence self-association processes by stacking at high concentrations and the presence of intra- and intermolecular hydrogen bonds, which are able to affect the molecular motion of both molecules.[25] In particular for rifaximin OR the intramolecular H-bonds are responsible for the stabilization of the aliphatic chain.[25]

Combined use of NMR experimental results, theoretical simulation of two-dimensional NMR spectra by complete relaxation matrix analysis (CORMA)[26] and molecular dynamics calculations,[27,28] represents a powerful approach in the determination of the structure of organic compounds in solution.

Geometrical constraints were obtained from both ROESY cross-peak intensities using the MARDIGRAS program[27] and selective proton–carbon nuclear Overhauser effects ({H}C-NOEs).[29–31] The derived proton–proton and proton–carbon distances were used in the molecular dynamics simulations[32–35] and the accuracy of the final structures of rifaximin and rifaximin OR was obtained generating the theoretical ROESY spectra by CORMA program. The structure obtained for rifaximin was compared to the crystal structure of rifamycin O reported by Bacchi et al.[10] in order to highlight the structural differences between a nonactive conformation and an active one as we found was that of rifaximin. As expected, the main changes involved the position of the ansa chains with respect to the naphtho-furanone moiety as well as the orientation of O(9) and O(10).

We also analyzed the extent of the conformational rearrangements induced by the chemical modification made on rifaximin. Although the opening of the aliphatic chain did not cause a complete rearrangement of the structure of rifaximin OR, some interesting modifications of the position of the aliphatic chain with respect to the naphtho-furanone moiety were found.

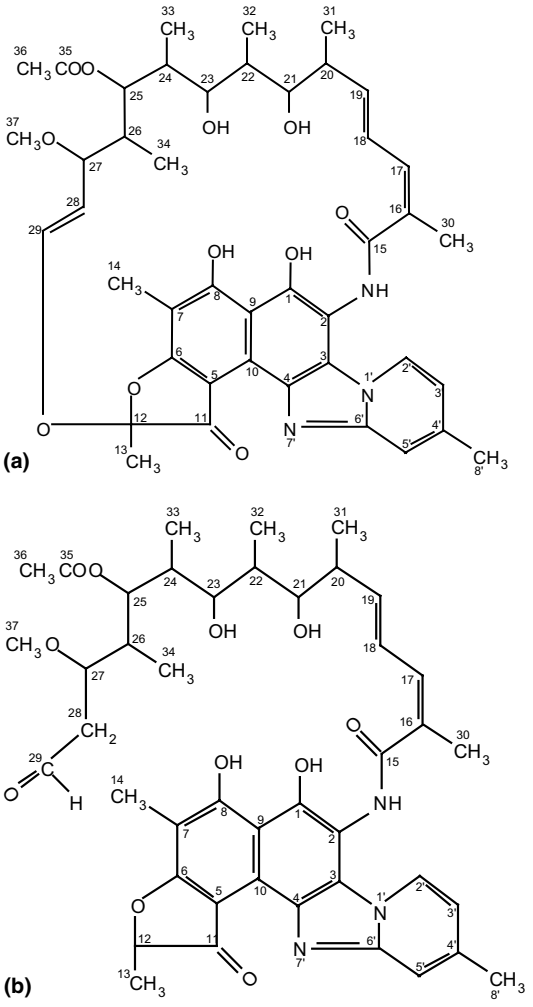

Chart 1. (a) Structure and numbering of rifaximin; (b) structure and numbering of rifaximin OR.

2. Results and discussion

2.1. Structural and dynamic information derived from NMR relaxation measurements

Proton and carbon-13 resonance assignments of rifaximin and rifaximin OR were shown in previous works.[24,25]

In order to gain information regarding relaxation mechanisms and molecular dynamics, an analysis of the observed nuclear Overhauser effects obtained after continuous broad band decoupling was performed. In Tables 1 and 2 carbon nuclei of rifaximin and rifaximin OR were divided into two groups, depending on the number of attached protons. Before the observed ^{13}C relaxation rates were interpreted in terms of molecular motions, the experimental broad band NOEs [NOE(BB)] were compared with the theoretical values expected for carbon nuclei totally relaxing through ^{1}H–^{13}C dipolar interactions. In the case of methyl groups, which are expected to satisfy the $(\omega_C + \omega_H) \ll 1$ motion conditions, the theoretical maximum value calculated for the NOE is equal to 1.99. Thus the fractional effectiveness of the dipolar relaxation for the methyl carbons is given by the ratio NOE(BB)/1.99. Values reported for both rifaximin and rifaximin OR (Tables 1 and 2) confirm that the methyl carbons relax mainly by dipole–dipole interaction with the attached proton nuclei. Tables 1 and 2 also show the experimental relaxation rate values measured for methine carbons belonging to the aliphatic chain and aromatic moiety of rifaximin and rifaximin OR. It can be noted that these relaxation rates assume higher values with respect to methyl carbons, due to slower molecular dynamics. Assuming that methine carbons relax predominantly by dipolar mechanism, a maximum theoretical NOE of 1.92 (which gave

Table 1. Observed and calculated relaxation parameters and NOEs for rifaximin in $CDCl_3$

C_nH_3	δ (ppm)	R_1 (s^{-1})	NOE(BB)/1.99	R_{1DD} (s^{-1})	$\tau_c \times 10^{10}$ (s)
8′	22.18	1.4	0.93	1.3	0.2
13	20.61	1.3	0.92	1.2	0.6
14	6.85	1.3	0.88	1.1	0.2
30	20.26	1.3	1.02	1.3	0.2
31	17.39	4.2	1.07	4.5	0.6
32	10.64	2.2	1.05	2.3	0.3
33	8.02	1.7	1.06	1.8	0.2
34	7.86	2.4	1.22	2.9	0.4
36	21.33	1.2	1.12	1.3	0.2
37	56.82	1.3	0.95	1.2	0.2
C_nH			NOE(BB)/1.92		
2′	128.22	7.8	0.98	7.7	4.4
3′	119.09	7.5	0.96	7.2	4.1
17	136.07	8.5	0.98	8.3	5.1
18	125.26	7.7	1.00	7.7	4.3
19	141.58	7.6	0.96	7.3	4.2
20	37.72	5.9	1.25	7.4	3.0
21	72.67	7.4	0.97	7.2	4.0
22	32.82	6.4	0.96	6.1	3.3
23	76.62	6.0	0.99	5.9	3.0
24	36.82	6.3	1.02	6.4	3.3
25	73.79	6.6	0.92	6.1	3.4
26	38.57	6.3	1.00	6.3	3.0
28	115.54	6.8	0.83	5.6	1.6
29	141.94	5.7	0.97	5.6	2.8

Table 2. Observed and calculated relaxation parameters and NOEs for rifaximin OR in $CDCl_3$

C_nH_3	δ (ppm)	R_1 (s^{-1})	NOE(BB)	NOE(BB)/1.99	R_{1DD} (s^{-1})	$\tau_c \times 10^{10}$ (s)
8′	22.6	1.7	2.03	1.02	1.7	0.2
13	17.6	4.1	1.99	1.00	4.1	0.6
14	7.3	1.6	1.88	0.95	1.5	0.2
30	21.7	1.8	2.35	1.18	2.1	0.3
31	17.0	3.7	2.40	1.21	4.5	0.5
32	12.0	2.1	2.24	1.13	2.4	0.3
33	9.7	1.6	2.21	1.11	1.8	0.2
34	10.8	1.7	2.35	1.18	2.0	0.2
36	21.5	1.2	2.14	1.08	1.3	0.2
37	58.5	1.0	1.93	0.97	1.0	0.2
C_nH				NOE(BB)/1.92		
2′	128.6	8.7	1.85	0.96	8.4	5.3
3′	118.0	9.5	1.92	1.00	9.5	6.4
17	138.2	8.4	1.90	0.99	8.3	5.0
18	127.8	9.6	1.94	1.01	9.7	6.5
19	144.3	9.8	1.60	0.83	8.2	6.7
20	41.2	8.5	2.24	1.17	9.9	5.1
21	74.8	6.3	1.91	0.99	6.3	3.2
22	34.1	6.1	1.85	0.96	5.9	3.1
23	77.9	6.7	1.87	0.97	6.5	3.4
24	37.9	7.8	1.94	1.01	7.9	4.4
25	74.9	6.3	1.73	0.90	5.7	3.2
26	39.0	5.1	1.95	1.02	5.2	2.5
27	76.0	4.7	1.96	1.02	4.8	2.3
28	46.9	3.4	1.64	0.85	2.9	0.7
29	201.5	0.9	1.98	1.03	0.9	0.4

the expected NOE(BB)/1.92 ratio of about 1) can be predicted. This maximum NOE corresponds to a correlation time of about 3.3×10^{-10} s, which can be considered as the correlation time for the skeleton of the two molecules.

The dipolar contribution to spin-lattice relaxation rates allowed the calculation of correlation time values modulating the ^{1}H–^{13}C interaction, assuming the proton–carbon distance equal to 1.08 Å.[36–39] τ_c values calculated for rifaximin and rifaximin OR are reported in column 6 of Table 1 and column 7 of Table 2. These values showed that the aromatic and diene regions of the two molecules experience slower reorientation motion than the aliphatic region. The aliphatic region of rifaximin showed similar values of correlation time, indicating a stable conformation of the molecule in solution despite of weak local dynamics. The aliphatic carbons of rifaximin OR showed correlation times similar to those of the aromatic carbons, except for the terminal aldehyde group, which experiences motions of the same magnitude as methyl groups. This suggests the existence of a partial rigidity of the aliphatic chain of rifaximin OR despite of the lack of the constraint existing in rifaximin structure. This stiffness vanishing at C28 and C29, represents an evidence of the high mobility of the terminal side of the aliphatic chain of rifaximin OR. In this analysis the contribution to the observed relaxation rates of aromatic carbons due to anisotropic reorientation was assumed to be negligible. This assumption was supported by the NOE values obtained for both aliphatic and aromatic carbons whose NOE_{exp}/NOE_{theor} value was close to unit. Correlation time values obtained from 13-carbon relaxation rate measurements were used in the MARDIGRAS algorithm for generating constraints bound.

2.2. Structural analysis

Before analyzing the through-space interactions, which enabled the identification of the conformational changes occurred after the brake of the aliphatic chain of rifaximin, a very interesting information was derived from the change in the $CH_3(34)$ proton chemical shift value observed for the two molecules shown in Figure 1. In particular, in the ^{1}H spectrum of rifaximin OR, $CH_3(34)$ resonance experienced a down-field shift of about 1.5 ppm, indicating that this group together with the aliphatic chain moved away from the shielding cone of the aromatic moiety. This was a first evidence of a change in the position of $CH_3(34)$ and therefore a preliminary indication of a structure rearrangement of the aliphatic chain of rifaximin OR.

2D-NOESY (nuclear Overhauser effect spectroscopy) experiments are usually used to identify spatial connectivities between nuclei, which are dipolarly coupled, since the size of the NOE depends inversely on the distance between two interacting spins.

Correlation time values calculated from carbon-13 longitudinal relaxation rates for rifaximin and rifaximin OR suggested that the $\omega_0\tau_c \ll 1$ motion condition does not apply for all carbons in the two systems.[25] For this reason the use of ROESY spectra to derive internuclear proton–proton distances seems to be more appropriate for studying this two biomolecules, considering that ROESY experiments are essential spin diffusion free.[40,41]

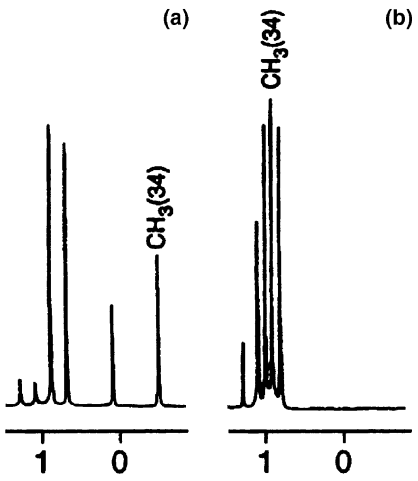

Figure 1. Portions of the proton spectra, which show the down-field shift of $CH_3(34)$ signal of rifaximin (a) with respect to rifaximin OR (b).

ROESY spectrum of rifaximin (Fig. 2) showed a number of predictable dipolar couplings (such as those between aromatic protons and some aliphatic chain protons), however some important interactions able to provide important information about the conformation were present. The most interesting dipolar connectivities obtained from ROESY spectrum of rifaximin are reported in Table 3.

In particular H2′–$CH_3(30)$, H2′–H18, and H2′–NH cross-peaks gave some crucial indications about distances between protons belonging to the aliphatic bridge and the aromatic moiety.

ROESY spectrum of rifaximin OR (Fig. 3) showed several other differences with respect to the rifaximin one. Table 3 shows the principal proton–proton dipolar interactions present in the ROESY spectrum of rifaximin OR. The presence of the H28b–$CH_3(14)$ interaction was an evidence of the shift of the aliphatic chain toward a more external position with respect to the aromatic moiety. At the same time this dipole–dipole interaction also indicated that the reduction process on the olefinic group of rifaximin did not cause a dramatic change in the molecular structure of rifaximin OR. Moreover, the presence of H28b–$CH_3(34)$ and H28b–$CH_3(14)$ cross-peaks showed that the molecular structure of rifaximin OR was not subject to strong conformational fluctuations. Other differences supporting the hypothesis of a structural rearrangement can be pointed out. In fact some proton–proton connectivities that can be found in rifaximin spectrum, as H17–$CH_3(31)$, were absent in rifaximin OR.

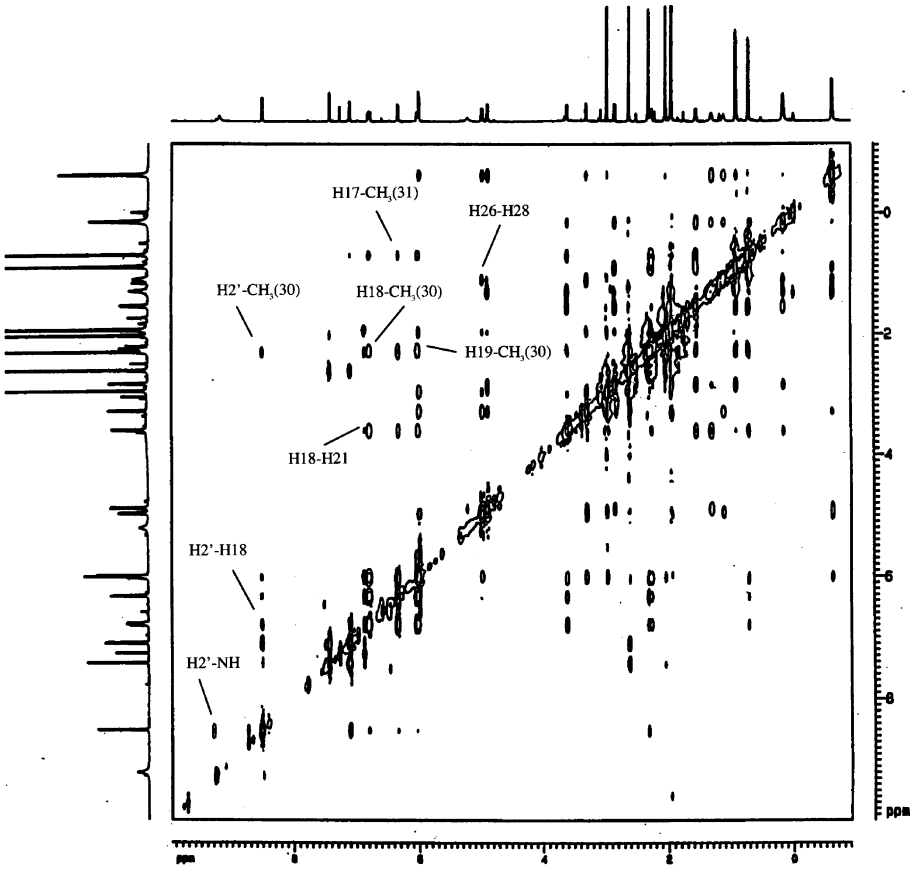

Figure 2. ROESY spectrum of rifaximin in $CDCl_3$ recorded at mixing time of 200 ms with the more interesting peaks indicated.

2.2.1. Extraction of geometrical constraints

2.2.1.1. Proton–proton internuclear distances. ROESY cross-peak intensities were used to calculate interproton distances for rifaximin and rifaximin OR using MARDIGRAS program. The most important source for obtaining information regarding conformational changes occurred after the break of the aliphatic chain of rifaximin, is represented by dipolar interactions between protons belonging to the aromatic moiety and the aliphatic chain for both biomolecules. For this reason we focused our attention to a set of cross-peaks, which in our opinion were able to clarify the extent of structural changes in rifaximin OR. These proton–proton interactions were H2′–CH_3(30), H2′–NH, H2′–H18, which were present in both molecules, and H28b–H34, H28b–H14 present only in rifaximin OR. In Table 4 the upper and lower bounds for the dipolar interactions are reported. We set the distance between H2′ and H3′ as fixed and known (equal to 2.49 Å) since it can be considered independent from the conformation.

Table 3. Close distances observed in the ROESY spectra of rifaximin and rifaximin OR

Rifaximin	Rifaximin OR
2′–30	2′–30
2′–NH	2′–NH
2′–18	—
—	12–13
17–31	—
18–21	—
18–30	—
18–31	18–31
19–20	19–20
19–21	19–21
19–30	—
—	24–31
26–28	—
26–34	26–34
26–33	26–33
27–28	—
—	27–28b
—	27–28a
28–29	—
—	28a–29
—	28b–29
—	28b–34
—	28b–14

2.2.1.2. Carbon–proton internuclear distances. Selective presaturation of a proton H_a, which interacts dipolarly through space with a ^{13}C nucleus C_b at a distance r_{ab} generates an NOE given by:[4]

$$\mathrm{NOE}_{C_b}(H_a) = \frac{\gamma_H}{\gamma_C}\frac{(W_2 - W_0)}{R_{C_b}}, \qquad (1)$$

where

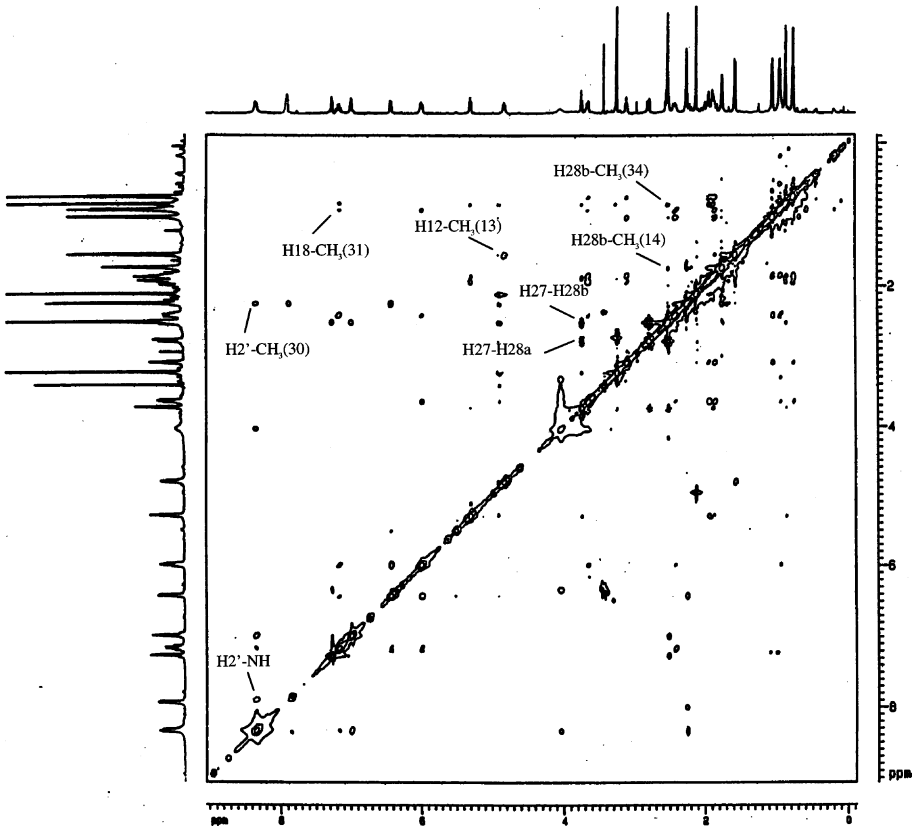

Figure 3. ROESY spectrum of rifaximin OR in $CDCl_3$ recorded at mixing time of 200 ms, which highlights the presence of $CH_3(14)$–H28b cross-peak and the lack of $CH_3(14)$–H28a cross-peak.

$$\frac{\gamma_H}{\gamma_C}(W_2 - W_0) = \sigma_{ab} = \frac{\hbar^2\gamma_H^3\gamma_C}{10r_{ab}^6}\left[\frac{6\tau_c}{1+(\omega_H+\omega_C)^2\tau_c^2} + \frac{\tau_c}{1+(\omega_H-\omega_C)^2\tau_c^2}\right] \quad (2)$$

and R_{C_b} is the spin-lattice relaxation rate measured for C_b under broadband decoupling conditions.

By combining selective NOE measurements and spin-lattice relaxation rates, information on proton–carbon distances can be obtained from the calculated cross-relaxation rates. If cross-relaxation rates are known, two independent methods can be used to determine proton–carbon internuclear distances.

Method A. When the saturation of H_a results in Overhauser effects on two or more carbon resonances, internuclear distances can be calculated from the following relation:

$$\frac{NOE_{C_1}(H_n)R_{C_1}}{NOE_{C_2}(H_n)R_{C_2}} = \frac{r_{C_2-H_n}^6}{r_{C_1-H_n}^6}. \quad (3)$$

In order to be able to evaluate distances from Eq. 3, no prior knowledge of correlation time is required, but one of the two distances, which has to be independent from the conformation or molecular motion, needs to be known for calibration.

Method B. If both correlation time τ_c and σ can be determined, an absolute calculation of carbon–proton distances can be performed using the following equation:

$$r_{ab}^6 = \frac{\hbar^2\gamma_H^3\gamma_C}{10NOE_{C_b}(H_a)R_{C_b}}\left[\frac{6\tau_c}{1+(\omega_H+\omega_C)^2\tau_c^2} + \frac{\tau_c}{1+(\omega_H-\omega_C)^2\tau_c^2}\right]. \quad (4)$$

In this work we used both of these methods, providing a double check on the calculated carbon–proton distances and the assumptions involved.

Table 5 reports some carbon–proton distances calculated with methods A and B for rifaximin and rifaximin OR.

2.2.2. Molecular dynamics calculations. The upper and lower bounds for proton–proton distances calculated with the MARDIGRAS algorithm together with carbon–proton distances obtained from selective {H}C-NOEs, were used in the restrained molecular dynamics (rMD)

Table 4. Upper and lower bounds determined by MARDIGRAS calculation for interproton distances

Protons	Upper–lower bounds (Å)	
	Rifaximin	Rifaximin OR
2′–30	2.60–2.30	3.74–3.50
2′–NH	2.16–1.80	2.73–2.47
2′–18	4.79–4.39	4.76–4.44
31–18	4.77–4.41	3.75–3.39
30–18	4.89–4.63	—
18–21	4.13–3.85	—
17–18	3.28–2.96	3.75–3.45
31–17	4.86–4.56	—
30–17	2.50–2.28	2.62–2.32
21–17	5.10–4.70	—
17–19	2.71–2.41	2.82–2.50
31–19	3.06–2.68	3.56–3.22
19–20	3.25–2.95	3.37–2.97
19–30	4.95–4.63	—
19–21	2.83–2.51	2.60–2.32
29–28	3.28–2.88	—
28–26	2.91–2.61	—
28–27	2.56–2.26	—
29–28b	—	2.68–2.38
29–28a	—	3.25–2.99
29–27	—	3.39–3.01
27–28b	—	2.67–2.27
27–28a	—	3.30–2.94
28a–28b	—	1.96–1.68
28b–34	—	3.43–3.19
28b–14	—	4.11–3.87
12–13	—	2.69–2.41
26–27	2.70–2.38	2.59–2.35
27–37	2.87–2.59	2.54–2.16
20–31	3.22–2.86	2.69–2.43
26–34	2.69–2.45	2.58–2.34
26–33	2.35–2.05	3.28–3.04

Table 5. Proton–carbon distances for (a) rifaximin and (b) rifaximin OR obtained from ^{1}H–^{13}C NOEs using methods A (r_A) and B (r_B)

Carbon	C*n*{NH}		C*n*{H2′}		C*n* {H3′}	
	r_A	r_B	r_A	r_B	r_A	r_B
(a)						
2′	—	2.7	—	—	2.2[a]	2.1[a]
3′	—	4.0	2.1[b]	2.1[b]	—	—
30	—	2.2	3.1	3.2	4.0	4.0
(b)						
2′	—	3.0	—	—	2.2[a]	2.2[a]
3′	—	4.2	2.2[b]	2.2[b]	—	—
30	—	2.2	4.3	4.3	—	—

[a] Calibrating distance for method A C2′–H3′ = 2.16 Å and correlation time for method B $\tau_c = 3.3 \times 10^{-10}$ s.
[b] Calibrating distance C3′–H2′ = 2.13 Å and correlation time for method B $\tau_c = 3.3 \times 10^{-10}$ s.

simulations of rifaximin and rifaximin OR in the presence of the solvent ($CDCl_3$).

Figure 4a and b shows the time course of the 1 ns MD simulation regarding the trajectories of the NH–C15–C16–C17 dihedral angle of rifaximin and rifaximin OR, respectively. Both angles oscillated in a narrow range, indicating that during the simulations no strong conformational changes regarding the aliphatic chain were observed in the two molecules. Even if this result was expected and obvious for rifaximin, in which the aliphatic chain links two opposite sides of the aromatic moiety, this represents an evidence of the stability of the open ring in rifaximin OR.

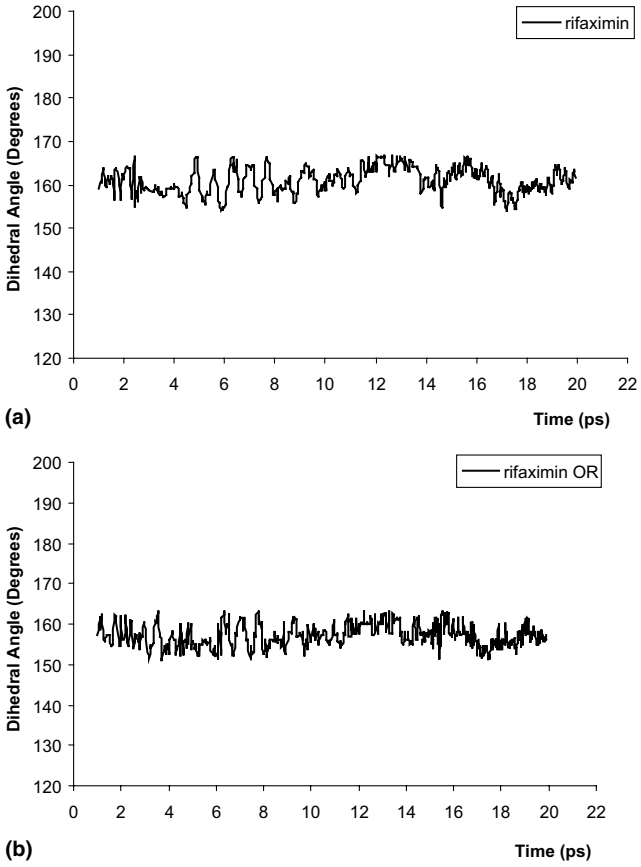

Figure 4. Time course of the 1 ns MD simulation regarding the trajectories of the NH–C15–C16–C17 dihedral angle of (a) rifaximin and (b) rifaximin OR.

The accuracy of the final structures obtained after MD simulations can be obtained with the calculation of the theoretical spectra within CORMA program. The fitting of the simulated spectra with experimental intensities was evaluated by crystallographic-type R_{NMR} factor defined in Section 4. Value of R_{NMR} for rifaximin and rifaximin OR was found to range from 0.21 to 0.25 for rifaximin (150 random snapshot of the 1 ns MD) and from 0.20 to 0.24 for rifaximin OR. These data indicate that the accuracy of the structures obtained from molecular dynamics simulations is good. Figure 5a and 5b shows the conformations of rifaximin and rifaximin OR resulting from full energy minimization of the structures obtained from MD calculations. The structure of rifaximin showed a conformation in which O(9) and O(10) were pointing outside the ring, following the qualitative model proposed by Arora.[14] Moreover, it seems clear that the opening of the aliphatic chain of rifaximin, which gave rise to rifaximin OR, did not cause a complete rearrangement of the structure of the molecule. In Figure 5b the hydrogen bonds present in

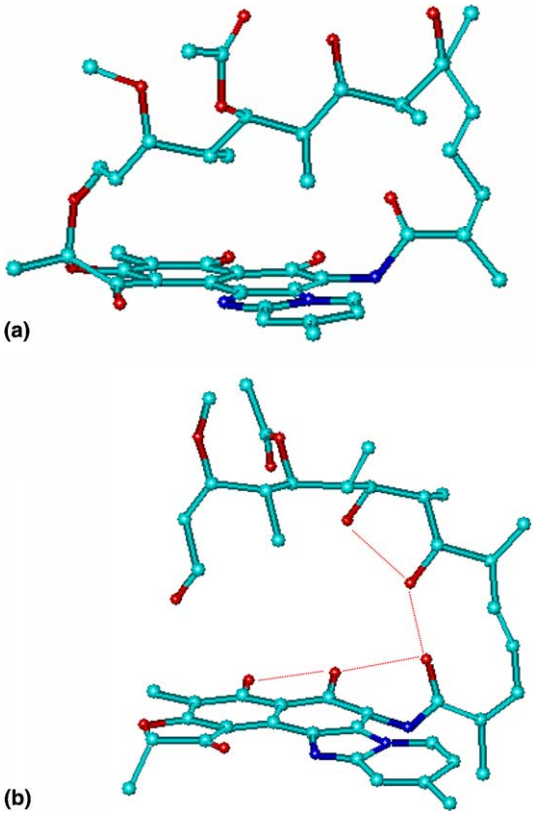

Figure 5. Conformations resulting from full energy minimization of the structures obtained from MD calculations of (a) rifaximin and (b) rifaximin OR (hydrogens omitted for clarity).

rifaximin OR are shown; in particular it is important to emphasize that we observe an H-bond between the carbonyl group C(15) and the hydroxyl group OH(21), which may be responsible for the stabilization of the aliphatic chain.

Figure 6 shows the superposition of the refined structure of rifaximin with the X-ray structure of rifamycin O reported in the paper by Bacchi et al.[10] obtained from Cambridge Crystallographic Data Centre (CCDC).[42] Since the antibiotic activity of rifamycins has been correlated to the conformation of the ansa chain, it is of interest to compare the structure of rifaximin with the crystal structure of rifamycin O. As expected, the main structural differences involved the ansa backbone of the two molecules, in particular regarding the central section from C19 to C29, including the orientation of O9 and O10, which in rifaximin were directed outside the ring while in rifamycin O pointed toward the naphthoquinone. As pointed out in Section 1, the orientation of O9 and O10 represents the main conformational characteristic in order to discriminate between active and nonactive structures, as proposed by Arora.[14] This findings are in perfect agreement with the results reported in the literature,[10,12] which state that the rotation of the ansa central segment C20–C26 around the dihedral angles C18–C19–C20–C21 and C25–C26–C27–C28 and a local rearrangement of the C21–C22–C23–C24 segment determine the active pattern for the pharmacophore (O1, O2, O9, O10).

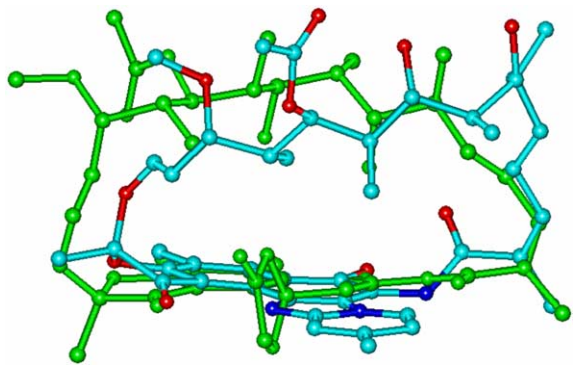

Figure 6. Overlay of the solution structure of rifaximin and the crystal structure of rifamycin O (green).

Another important structural difference involves the position of $CH_3(34)$, which in rifaximin points toward the aromatic moiety. This is in perfect agreement with $CH_3(34)$ chemical shift value, which was found to be −0.6 ppm, suggesting a strong shielding effect due to the aromatic π system on the methyl group. On the contrary, in rifamycin O, $CH_3(34)$ is oriented outside the ring due to the presence of the oxolanone 4-substituent, which lies almost perpendicular to the chromophore plane. In this case, literature data report a chemical shift value of 0.20 ppm.[10]

3. Conclusions

In this work, the conformational properties of two related compounds, rifaximin and rifaximin OR, were studied by experimental NMR and theoretical simulation methods. Rifaximin was found to be in an active conformation according to the model reported in the literature. The reduction process on rifaximin caused the break of the aliphatic chain, which was found to be no longer symmetrical with respect to the naphtho-quinonic plane. Even though this chemical modification was expected to cause strong rearrangements of the aliphatic chain, NMR analysis, MD and MM simulations put in evidence that no dramatic structural rearrangements occurred.

4. Experimental

Rifaximin, 4-deoxy-4′-methylpyrido-(1′2′-1,2)-imidazo-(5,4*c*)rifamycin SV was purchased from Alfa Wassermann S.p.A. (Bologna, Italy) and used without any further purification. Rifaximin OR (open ring) was obtained by electrolytic reduction of rifaximin.[24]

4.1. NMR methods

2D-NMR experiments were performed with a Bruker DRX-600 Avance spectrometer operating at 600.13 MHz for ^1H, equipped with an *xyz* gradient unit. As probe heads we used a reverse triple resonance (^1H,

^{13}C, BB) probe with *xyz* gradients for two-dimensional experiments.

Rotating frame NOESY (ROESY)[43] were acquired with 2048 complex points for 256 experiments with 10 s recycle delay and time proportional phase incrementation (TPPI) phase cycle. ROESY spectra were acquired in $CDCl_3$ as solvent with mixing times of 200 ms.

Data were processed with XWINNMR software (Bruker), and 2D spectra were analyzed with SPARKY software.[44] Integration of cross-peak volumes in the ROESY spectra were done using the Gaussian-fitting algorithm of SPARKY and the necessary offset corrections were performed with the program.

A Varian XL-200 spectrometer operating at 200 and 50.3 MHz for proton and carbon nuclei, respectively, was used for recording ^{1}H and ^{13}C spectra. Carbon-13 relaxation rates were measured by using the standard inversion recovery $(180°–\tau–90°–AQ)_n$ pulse sequence. A 5% experimental error was estimated for the relaxation rate values. Nonselective broad-band NOEs were measured by comparing peak intensities obtained in fully and gated decoupled ^{13}C spectra. Selective heteronuclear NOEs were generated by presaturating, with a low power decoupler pulse, single proton resonances;[4] the duration of this decoupler pulse was set 10 times the relaxation time of the irradiated proton to get a full NOE; a high power decoupler pulse during the 90° ^{13}C pulse and the acquisition time yielded fully proton decoupled ^{13}C spectra with only selective NOEs; a delay 5 times longer than the longest ^{13}C relaxation time was used to allow a complete relaxation of the spin system. Constraints bound were generated with MARDIGRAS algorithm, which was a complete relaxation matrix approach, assuming overall isotropic molecular motion. Hybrid relaxation matrices were built using cross-peak volumes of the 200 ms spin lock ROESY intensities assuming an isotropic correlation time of 3.3×10^{-10} s.[25] As starting model for MARDIGRAS calculations the final structures of a preliminary unrestrained molecular dynamics (MD) and subsequent full energy minimization were used. MARDIGRAS can account for the offset dependence of the transverse relaxation in the rotating frame and for the homo-nuclear Hartmann–Hahn (HOHAHA) distortion of the intensities, giving the carrier frequency and coupling constants, respectively. To take in account integrations errors, we used a procedure that calculates final upper and lower bound from a statistical set of bounds generated by a series of MARDIGRAS runs in which user-defined percentage error is randomly added on top of an absolute noise errors RAND-MARDI.[45] Here 500 random distance bound sets were created, using 10% as the minimum percentage error for all intensities, and an absolute noise error equal to the smallest peak.

4.2. Molecular modeling and structure refinement

Molecular dynamics simulations were performed with MACROMODEL 5.0 program,[46] on Silicon Graphics (SGI), INDIGO 2 Solid Impact working under IRIX 6.3 operating system. The rMD calculations were conducted using a solvation model, which treats the solvent ($CDCl_3$) as an analytical continuum starting near the van der Waals surface of the solute.[47] In calculations using continuum solvation, the program uses an approximate solvent accessible surface area function for derivatives and then computes final energies with a more exact area function at the end of calculation. The protocol for simulated annealing calculations were: (i) equilibration period of 10 ps at 10 K; (ii) annealing by heating to 700 K in 50 ps; (iii) maintaining at 700 K for 50 ps; (iv) cooling at 10 K in 10 ps. Experimental constraints were applied for the total duration of the simulation. The systems (rifaximin and rifaximin OR) obtained at the end of the simulated annealing were subject to energy minimization without constraints. In the refinement procedure the accuracy of the models obtained after molecular dynamics calculations was evaluated on the basis of the R_{NMR} factor, comparing experimental and theoretical ROESY spectra calculated from the following equation:[48]

$$R_{NMR} = \frac{\sum_{i,j,m} W_{ij}(\tau_m)|I_{ij}^{calc}(\tau_m) - I_{ij}^{exp}(\tau_m)|}{\sum_{i,j,m} W_{ij}(\tau_m) I_{ij}^{exp}(\tau_m)}, \qquad (5)$$

where I_{ij} are the NOE intensities for the i and j atoms (with $i \neq j$), τ_m is the mixing time, and $W_{ij}(\tau_m)$ are the weights in order to lower the effects of the experimental error.

Acknowledgement

The authors would like to thank the CSGI for financial support.

References and notes

1. Ceccato, M.; Lo Nostro, P.; Rossi, C.; Bonechi, C.; Donati, A.; Baglioni, P. *J. Phys. Chem. B* **1997**, *101*, 5094.
2. Donati, A.; Rossi, C.; Martini, S.; Ulyanov, N. B.; James, T. L. *Appl. Magn. Reson.* **1998**, *15*, 401.
3. Schmitz, U.; Donati, A.; James, T. L.; Ulyanov, N. B.; Yao, L. *Biopolymers* **1998**, *46*(5), 329.
4. Niccolai, N.; Rossi, C.; Brizzi, V.; Gibbons, W. A. *J. Am. Chem. Soc.* **1984**, *106*, 5732.
5. Niccolai, N.; Rossi, C.; Mascagni, P.; Gibbons, W. A.; Brizzi, V. *J. Chem. Soc., Perkin Trans. 1* **1985**, 239.
6. Brizzi, V.; Brufani, M.; Cellai, L.; Segre, A. L. *J. Antibiot.* **1983**, *36*, 516.
7. Oppolzer, W.; Prelog, V. *Helv. Chim. Acta* **1973**, *56*, 2287.
8. Brufani, M.; Cellai, L.; Cerrini, S.; Fedeli, W.; Marchi, E.; Segre, A.; Vaciago, A. *J. Antibiot.* **1984**, *37*(12), 1623.
9. Cellai, L.; Cerrini, S.; Segre, A. *J. Org. Chem.* **1982**, *47*, 2652.
10. Bacchi, A.; Pelizzi, G.; Nebuloni, M.; Ferrari, P. *J. Med. Chem.* **1998**, *41*, 2319.
11. Casey, M. L.; Whitlock, H. W. *J. Am. Chem. Soc.* **1975**, *97*, 6231.
12. Bacchi, A.; Pelizzi, G. *J. Comput. Aided Mol. Des.* **1999**, *13*, 385.
13. Arora, S. K. *J. Med. Chem.* **1985**, *28*, 1099.

14. Arora, S. K. *Mol. Pharmacol.* **1983**, *23*, 133.
15. Wehrli, W.; Knosel, F.; Schmid, K.; Staehlin, M. *Proc. Natl. Acad. Sci. U.S.A.* **1968**, *61*, 667.
16. Thompson, F. M.; Tischler, A. N.; Adams, J.; Calvin, M. *Proc. Natl. Acad. Sci. U.S.A.* **1974**, *71*, 107.
17. Lancini, G.; Zanichelli, W. In *Structure Activity Relationships Among the Semisynthetic Antibiotics*; Perlmann, D., Ed.; Academic: New York, 1977; pp 531–600.
18. Brufani, M.; Cellai, L.; Marchi, E.; Segre, A. L. *J. Antibiot.* **1984**, *37*, 1611.
19. Cellai, L.; Cerrini, S.; Segre, A. L.; Battistoni, C.; Cossu, G.; Mattogno, G.; Brufani, M.; Marchi, E.; Venturini, A. P. *Farmaco* **1989**, *44*, 97.
20. Cellai, L.; Heumann, H.; Baer, G.; Werel, W. *Eur. J. Med. Chem.* **1989**, *24*, 105.
21. DuPont, H. L.; Ericsson, C. D.; Cabada, F. J. *Digestion* **1998**, *59*(6), 708.
22. Di Stefano, M.; Malservisi, S.; Corazza, G. R. *Aliment. Pharm. Therap.* **2000**, *14*(5), 551.
23. Brufani, M. In *Topics in Antibiotic Chemistry*; Sammes, P. G., Ed.; Ellis Horwood: Chichester, 1977; pp 91–217.
24. Rossi, C.; Marchettini, N.; Bonechi, C.; Donati, A.; Corbini, G.; Corti, P. *J. Chem. Res. S* **1996**, *6*, 268.
25. Martini, S.; Magnani, A.; Corbini, G.; Corti, P.; Lampariello, R.; Ricci, M.; Picchi, M. P.; Bonechi, C. *Spectrosc. Lett.* **2002**, *35*(4), 581–602.
26. Keepers, J. W.; James, T. L. *J. Magn. Reson.* **1984**, *57*, 404–426.
27. Borgias, B. A.; James, T. L. *J. Magn. Reson.* **1990**, *87*, 475–487.
28. Karplus, M.; Petsko, G. A. *Nature* **1990**, *347*, 631.
29. Uzawa, J.; Takeuchi, S. *Org. Magn. Reson.* **1978**, *11*, 502.
30. Aldersley, M. F.; Dean, F. M.; Mann, B. F. *J. Chem. Soc., Chem. Commun.* **1983**, 107.
31. Ford, J. J.; Gibbons, W. A.; Niccolai, N. *J. Magn. Reson.* **1982**, *47*, 522.
32. Boelens, R.; Koning, T. M. G.; Kaptein, R. *J. Mol. Struct.* **1988**, *173*, 299.
33. Baleja, J. D.; Moult, J.; Sykes, B. D. *J. Magn. Reson.* **1990**, *87*, 375.
34. Kirkpatrick, S.; Gelatt, C. D., Jr.; Vecchi, M. P. *Science* **1983**, *220*, 4598.
35. Aramini, J. A.; Mujeeb, A.; Ulyanov, N. B.; Germann, M. W. *J. Biomol. NMR* **1990**, *18*, 287.
36. Wehrli, F. W.; Wirthlin, T. *Interpretation of Carbon-13 NMR spectra*; Heyden and Son: London, 1976.
37. Allerhand, A.; Kormorski, R. A. *J. Am. Chem. Soc.* **1973**, *95*, 8828.
38. Kormorski, R. A.; Peat, I. R.; Levy, G. C. *Biochem. Biophys. Res. Commun.* **1975**, *65*, 272.
39. Norton, R. S.; Allerhand, A. *J. Am. Chem. Soc.* **1976**, *98*, 1007.
40. Noggle, J. H.; Schirmer, R. E. *The Nuclear Overhauser Effect*; Academic: New York, 1971.
41. Neuhaus, D.; Williamson, M. *The Nuclear Overhauser Effect in Structural and Conformational Analysis*; VCH: New York, 1989.
42. Allen, F. H.; Kennard, O. *Chem. Des. Autom. News* **1993**, *8*, 1 and 31.
43. Bothner-By, A. A.; Stephens, R. L.; Lee, J.; Warren, C. D.; Jeanloz, R. W. *J. Am. Chem. Soc.* **1984**, *106*, 811–813.
44. SPARKY program for NMR assignment and integration, Computer Graphics Laboratory, University of California, San Francisco, USA.
45. Liu, H.; Spielmann, P.; Ulyanov, N. B.; Wemmer, D. E.; James, T. L. *J. Biomol. NMR* **1995**, *6*, 390–402.
46. Mohamadi, F.; Richards, N. G. J.; Guida, W. C.; Liskamp, R.; Lipton, M.; Caufield, C.; Chan, G.; Hendrickson, T.; Still, W. C. *J. Comput. Chem.* **1990**, *11*, 440.
47. Clark Still, W.; Tempczyk, A.; Hawley, R. C.; Hendrickson, T. *J. Am. Chem. Soc.* **1990**, *112*, 6127.
48. Gonzales, C.; Rullmann, J. A.; Bonvin, A. M. J. J.; Bolens, R.; Kaptein, R. *J. Magn. Reson.* **1991**, *91*, 659–664.